Journal of Power Sources 196 (2011) 8197–8206

Contents lists available at ScienceDirect

Journal of Power Sources

journal homepage: www.elsevier.com/locate/jpowsour

Investigation on the effect of microstructure of proton exchange membrane fuel cell porous layers on liquid water behavior by soft X-ray radiography

Takashi Sasabe*, Phengxay Deevanhxay, Shohji Tsushima, Shuichiro Hirai

Department of Mechanical and Control Engineering, Tokyo Institute of Technology 2-12-1, O-okayama, Meguro-ku, Tokyo 152-8552, Japan

ARTICLE INFO

Article history:
Received 7 January 2011
Received in revised form 4 May 2011
Accepted 17 May 2011
Available online 1 June 2011

Keywords:
Soft X-ray radiography
In situ diagnostics
GDL microstructure
Micro porous layer
Liquid water behavior
PEMFC

ABSTRACT

In order to investigate the effect of microstructure of PEMFC porous layers on the liquid water transport, liquid water accumulation and discharge behavior in the operating PEMFC was visualized by laboratory-based soft X-ray radiography. The utilization of low energy X-ray made it possible to visualize the liquid water behavior in the PEMFC with the spatial resolution of 0.8 μm and the temporal resolution of 2.0 s frame^{-1}, and the cross-sectional imaging can resolve the each components of the PEMFC. The visualization results showed that adding the MPL prevents the accumulation of liquid water in the substrate layer from contacting and forming the liquid water film on the catalyst layer. Furthermore, it was found that the liquid water distribution in the carbon paper and the carbon cloth GDL was completely different. The liquid water in the carbon cloth GDL concentrates at the weaves of fiber bundle and was effectively discharged to the channel. These visualization results suggested that the microstructure of the PEMFC porous layers strongly affect the liquid water behavior in the PEMFC, and the detailed understanding of the pore structures and the network of liquid water is essential for keeping the oxygen transport path to the catalyst site.

1. Introduction

The proton exchange membrane fuel cell (PEMFC) is regarded as a promising alternative clean power source for automobiles. Among the key issues for the acceptance of PEMFC for automobiles, cost reduction and improvement of power density for the downsizing of the PEMFC stack are needed. In order to meet these demands, further improvements of cell performance under high current density is required. The condensation of the produced water can be expected to occur under high current density operation. While a humidified environment is beneficial for the membrane conductance, the saturation of the pores in the catalyst layer (CL) and the gas diffusion layer (GDL) with liquid water might impede the transport of the reactants to the catalyst site. This phenomenon known as "flooding" is an important limiting factor of the PEMFC performance under high current density condition. Therefore, a fundamental understanding of the liquid water behavior in the PEMFC porous layers is essential for the further improvement of the PEMFC performance.

To elucidate the liquid water behavior in the operating PEMFC, a number of numerical models [1–7] have been reported. The numerical models can be classified into the macroscopic and the microscopic model. The macroscopic model [1–4] is based on the theory of volume averaging and treat the CL and GDL as macro-homogeneous porous layers. The macroscopic model is computationally more efficient and can be used for the entire cell model. However, because of the macroscopic nature, the macroscopic model fails to resolve the influence of the structural morphology of the CL and GDL. The microscopic modeles [5–7], which combines the microstructure and the transport phenomena, is attracted attention to elucidate the structure–transport interractions in the PEMFC porous layers. Though the detailed understandings are increasingly obtained by numerical models, the lack of experimental validation is a crucial problem. Therefore, in situ imaging techniques such as direct optical visualization, neutron radiography (NRG), and X-ray radiography are helpful for understanding the liquid water behavior in the PEMFC porous layers. Optically transparent cell [8,9] can permit the direct visualization of the liquid water behavior in the PEMFC with high temporal and spatial resolution. However, due to the opaque nature of the GDL and the bipolar plate, it is difficult to visualize the liquid water behavior within the GDL. NRG [10–13] can visualize and quantify the liquid water in the PEMFC porous layers, and the cross-sectional imaging (cell membrane parallel to the beam) can resolve the liquid water distribution between the different layers composing a cell [11,12]. Though the maximum spatial resolution of NRG is relatively high (13 μm) [13], enhanced spatial resolution requires long image-to-image times in the range of several minutes, and it

* Corresponding author. Tel.: +81 3 5734 3554; fax: +81 3 5734 3554.
E-mail address: sasabe.t.ab@m.titech.ac.jp (T. Sasabe).

0378-7753/$ – see front matter © 2011 Elsevier B.V. All rights reserved.
doi:10.1016/j.jpowsour.2011.05.045

was difficult to visualize the transient behavior of the liquid water in the operating PEMFC. In addition, NRG has a high sensitivity to the liquid water but not sensitive to the carbon and other materials used in the PEMFC. Due to the limited resolution and contrast, the GDL is invisible, and it was difficult to study the influence of the GDL microstructure on liquid water behavior by NRG. X-ray radiography is sensitive to both the liquid water and the carbon, and it has been used in soil science and petroleum industry to obtain structural information and to image fluid transport in reservoir rocks. Sinha et al. [14] demonstrated X-ray microtomography to measure the liquid water distributions in the GDL during with the spatial resolution of 10 μm. In addition, Koido et al. [15] demonstrated the microfocal X-ray CT and successfully visualized the microstructure of the carbon paper GDL with the spatial resolution of 1 μm.

Synchrotron X-ray imaging is a novel approach for the visualization of liquid water behavior in the operating PEMFC. Hartnig et al. [16,17] demonstrated synchrotron X-ray radiography and the results of cross-sectional imaging of the operating PEMFC with the spatial resolution of 3–7 μm were reported. To investigate the liquid water behavior in the operating PEMFC, NRG and synchrotron X-ray radiography are extremely useful techniques. However, the radiography technique with the neutron beam or the synchrotron X-ray can only be performed at the certain reactor sites. Therefore, the accessibility and the machine time are limited, and a laboratory-based instrument for immediate visualization of the liquid water in the operating PEMFC is needed in research and development cycles. To satisfy this demand, we have developed the soft X-ray microscopy system [18]. The system can be used in ordinary laboratories, and the liquid water accumulation and discharge behavior in the operating PEMFC were visualized with the spatial resolution of 1.0 μm and the temporal resolution of 1 s frame^{-1}.

Among the PEMFC components, the GDL has a large effect on the water transport. A bilayer GDL, consisting of a coarse substrate layer and a finer micro porous layer (MPL), has been employed to improve the PEMFC performance under high current density operation. The MPL typically consists of carbon powder bound

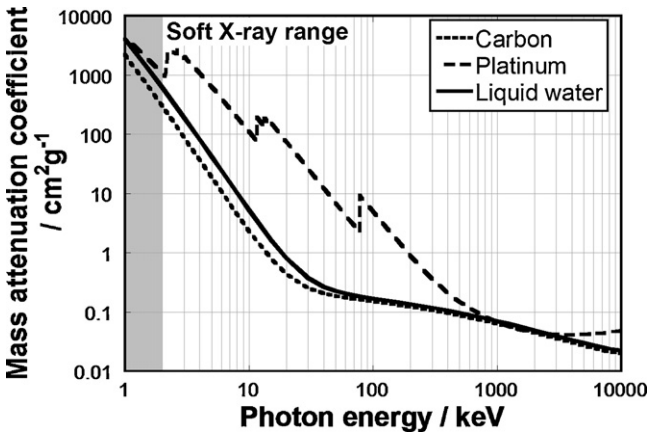

Fig. 1. The mass attenuation coefficients of water and selected elements used in the PEMFC.

with a hydrophobic polymer (e.g., polytetrafluoroethylene: PTFE). A number of researches has been made about the water transport through the MPL, but the actual function of the MPL is not fully understood. Some works [19,20] concluded that the MPL acts as a capillary barrier to water entering the cathode GDL and forces water to permeate from the cathode to the anode. However, other works [21,22] concluded that the MPL has no impact on back diffusion. In addition, two types of the substrate layer are commonly used in the PEMFC: carbon paper and carbon cloth GDL. Both of them are carbon–fiber-based materials, and the carbon paper GDL is non-woven, while carbon cloth GDL is woven fabric. It has been experimentally observed that a carbon cloth GDL displays better performance than a carbon paper GDL under humidified condition. Though a number of reports has been made, a relationship between the GDL microstructure and the performance is not fully understood. We have investigated the effect of the GDL microstructure on the liquid water accumulation behavior in the in-plane direction

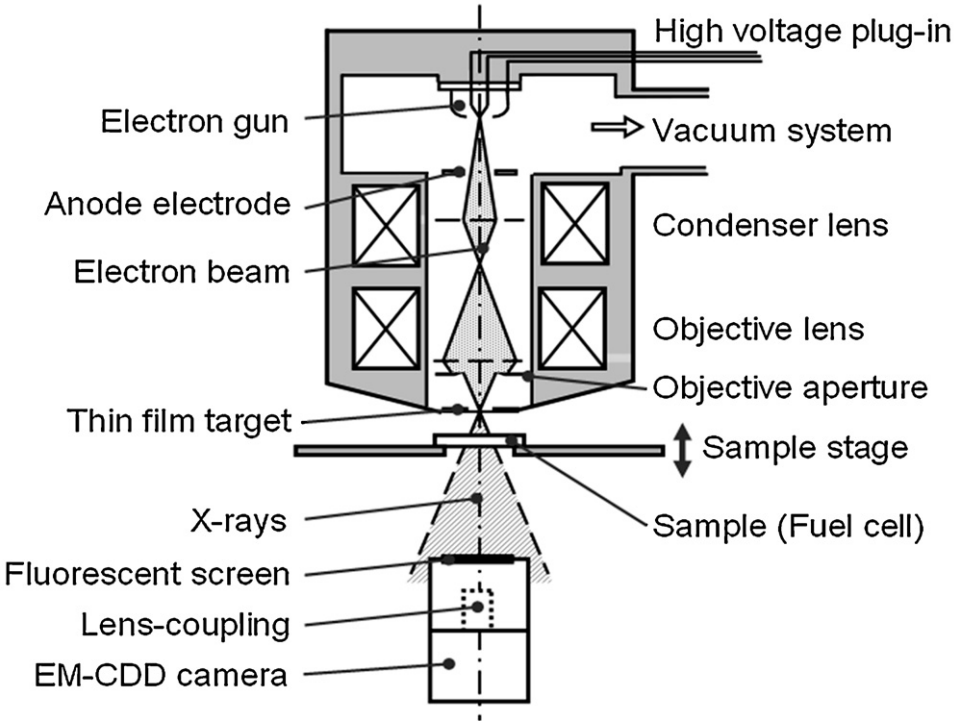

Fig. 2. Schematic of the soft X-ray microscopy system.

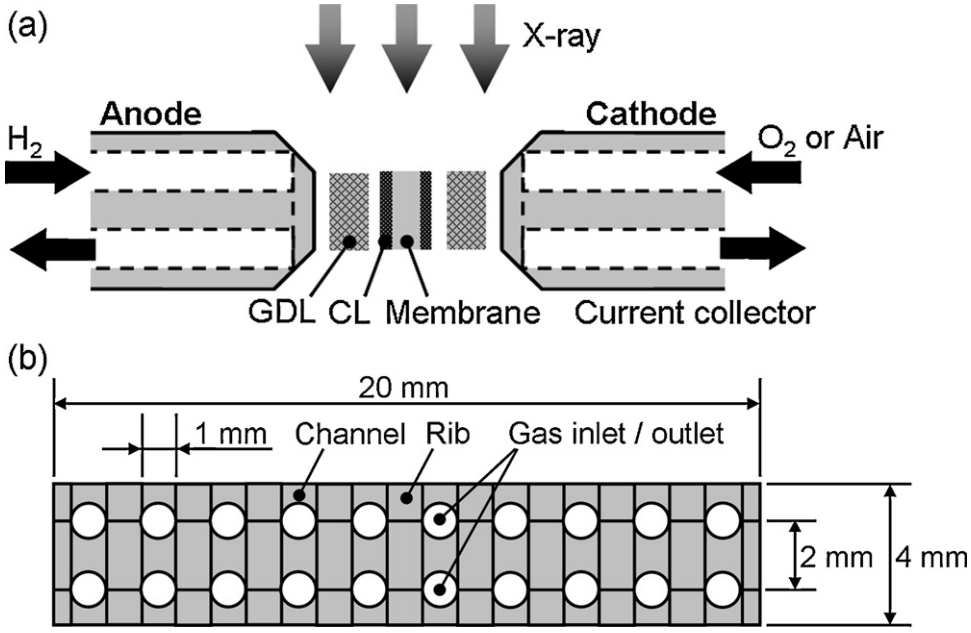

Fig. 3. Schematic of the cross-sectional imaging cell.

(cell membrane vertical to the X-ray beam), and the results showed that the liquid water distribution was completely different between the carbon paper and the carbon cloth GDL [23]. These results were highly beneficial for the understanding of liquid water behavior, but the imaging in the in-plane direction could not distinguish whether the liquid water reside in the anode or the cathode.

In this study, to investigate the effect of microstructure of porous layers on the liquid water transport in more detail, liquid water accumulation and discharge behavior in the operating PEMFC was visualized by soft X-ray radiography. The cross-sectional imaging can resolve the each components of the PEMFC, and the importance of detailed understanding of the porous structure and the network of liquid water was suggested.

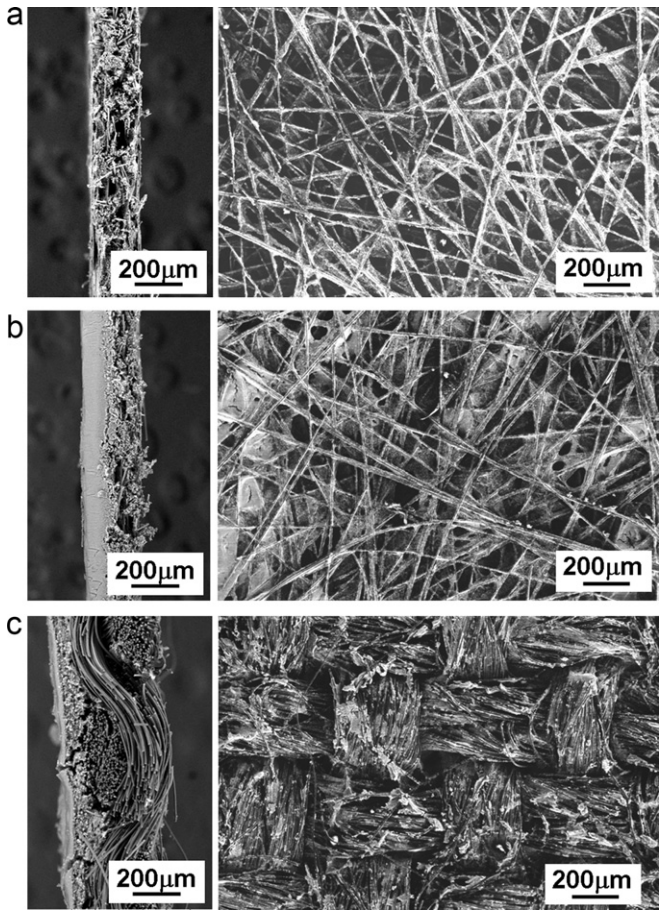

Fig. 4. Cross-sectional and surface SEM images of the GDLs. (a) SIGRACET® 24BA. (b) SIGRSCET® 24BC. (c) ELAT® LT1400-W.

2. Experimental

2.1. Soft X-ray radiography

Fig. 1 shows the mass attenuation coefficient of the materials used for PEMFCs. The photon energy of the conventional X-ray systems that are available in laboratories is generally in excess of 100 keV, and the mass attenuation coefficients of liquid water and carbon is much lower than that of platinum. Therefore, it had been considered that the visualization of the liquid water in the PEMFC would not be a suitable application for X-ray radiography technique. Meanwhile, the mass attenuation coefficients of Platinum and liquid water become closer in the range of low photon energy of less than 2.0 keV (soft X-ray range). Therefore, optimizing the wavelength of the X-rays (using the soft X-ray range) makes it possible to detect the liquid water in the PEMFC by X-ray radiography technique. The schematic of laboratory-based transmission soft X-ray microscope system (Tohken, TUX-3110FC) was shown in Fig. 2. Conventional hard X-ray microscope was modified to generate and detect the low energy X-ray. Unlike synchrotron X-ray radiography, the low energy X-ray generated from a thin-film target irradiated by an electron beam is not monochromated but consists of a broad spectrum of low energy X-rays. The low energy X-ray emerges from a point source in this instrument, and the technique is therefore inherently different from both NRG and synchrotron X-ray radiography, where a collimated beam is used. This feature has a potential advantage in terms of achieving a high spatial resolution, because large geometrical magnifications can be implemented. The sample (e.g., PEMFC) is placed near the X-ray source and the detector unit is located at a position distant from the X-ray source to give a large

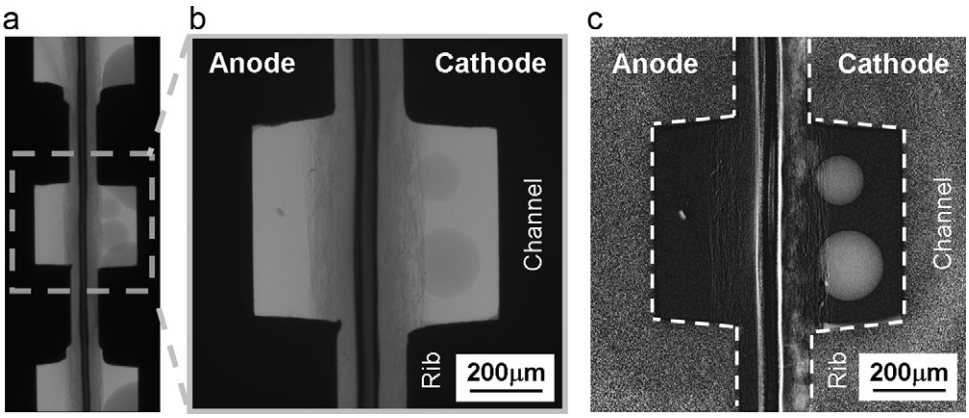

Fig. 5. Image normarizing process. (a) Low magnificatgion image; (b) high magnification image; and (c) normalized image.

geometrical magnification. In this study, the accelerating voltage of 15 kV was selected, and the spatial resolution of visualization was 0.8 μm.

2.2. Cross-sectional imaging cell

Schematic of the cross-sectional imaging cell is shown in Fig. 3. To permit the penetration of the low energy X-ray through the cell, the thickness (penetration length) of the cell was carefully decided, and an active area of the cell was set at 0.4 cm^2 (2 cm × 0.2 cm). The rib and channel widths were 1.0 mm, and the number of channels was 10.

2.3. Effect of MPL on liquid water behavior

To investigate the effect of adding the MPL on liquid water behavior, liquid water visualization tests were performed on two types of carbon paper GDLs with and without MPL. The detailed experimental conditions and the MEA specifications used in this study were summarized in Table 1. Two sheets of a Nafion® NRE211(thickness: 25 μm) were used for the polymer electrolyte membrane. The catalyst layers were hot-pressed on the membrane, and the catalyst loading was 0.25 mg Pt cm^{-2} for both the anode and the cathode. SIGRACET® 24BA (carbon paper, w/o MPL) and SIGRACET® 24BC (carbon paper, w/MPL) were used for both the anode and the cathode GDL, and the compression pressure of the cell was set at 1.0 MPa. Hydrogen and oxygen or air gases were used as the fuel and oxidant gas with the flow rates of 1.0 NL min^{-1}. To promote the water accumulation in the PEMFC, the cell was operated under the room temperature (25 °C), and the bubbler temperature was 20 °C (relative humidity: 72%). Though Reum et al. [24] reported the effect of cathode gas on current density distribution in the direction of rib and channel, significant difference in the liquid water distribution was not observed in operations with oxygen and air by soft X-ray radiography. Therefore, the following visualization tests were performed with pure oxygen gas.

Fig. 4 shows the scanning electron microscope (SEM) images of these two types of GDL. These materials had the same substrate layer and hydrophobic polymer content (5 wt%), while the 24BC GDL had the MPL. The MPL was shown on the left side of the 24BC GDL (Fig. 4(b)), and the thicknesses of the MPL was c.a. 100 μm.

Table 1
MEA specifications and operating conditions.

Parameter	Value
Membrane (thickness)	Nation® 211 (25.4 × 2 μm)
Catalyst layer (thickness)	Pt/C, 0.25 mgPt cm^{-2} (10 μm)
Gas diffusion layer	SIGRACET® 24BA (paper, w/o MPL) SIGRACET® 24BC (paper, w/MPL) ELAT® LT1400-W (cloth, w/MPL)
Compression pressure	1.0 MPa
Flow field	Straight channel (Rib/channel = 1.0/1.0 mm)
Cell temperature	25 °C
Relative humidity	72%
Reactant gas	Anode: hydrogen; cathode: oxygen, air
Gas flow rate	1.0 NL min^{-1} (dry)

2.4. Effect of GDL microstructure on liquid water behavior

To investigate the effect of the GDL microstructure on liquid water behavior, liquid water visualization tests were performed on the carbon paper and the carbon cloth GDLs. The experimental conditions and the MEA specifications were almost the same as summarized in Table 1. However, SIGRACET® 24BC and ELAT®

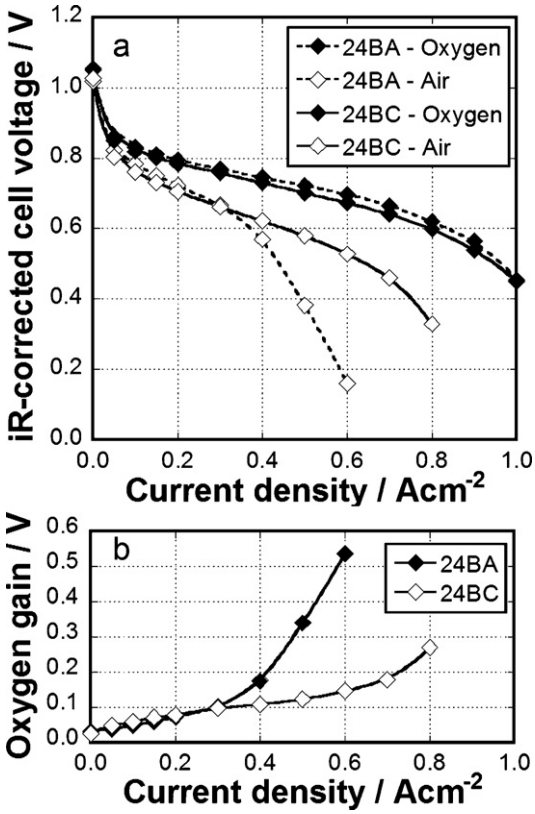

Fig. 6. Effect of adding the MPL on cell performance. (a) Polarization characteristics; and (b) oxygen gain.

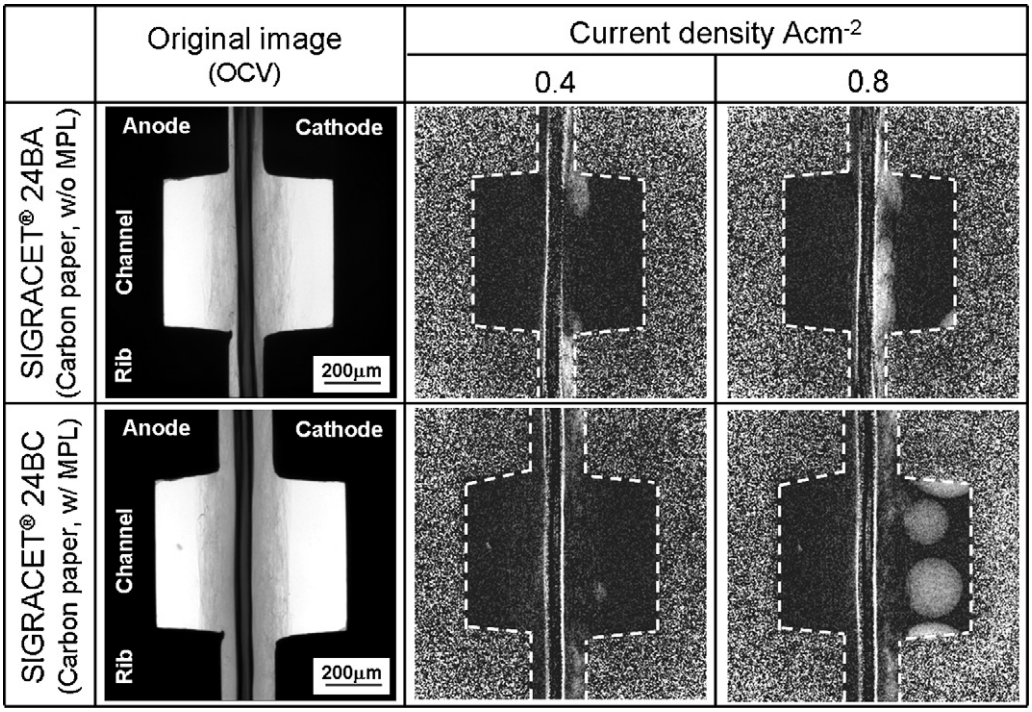

Fig. 7. Effect of current density on liquid water distribution in MEA.

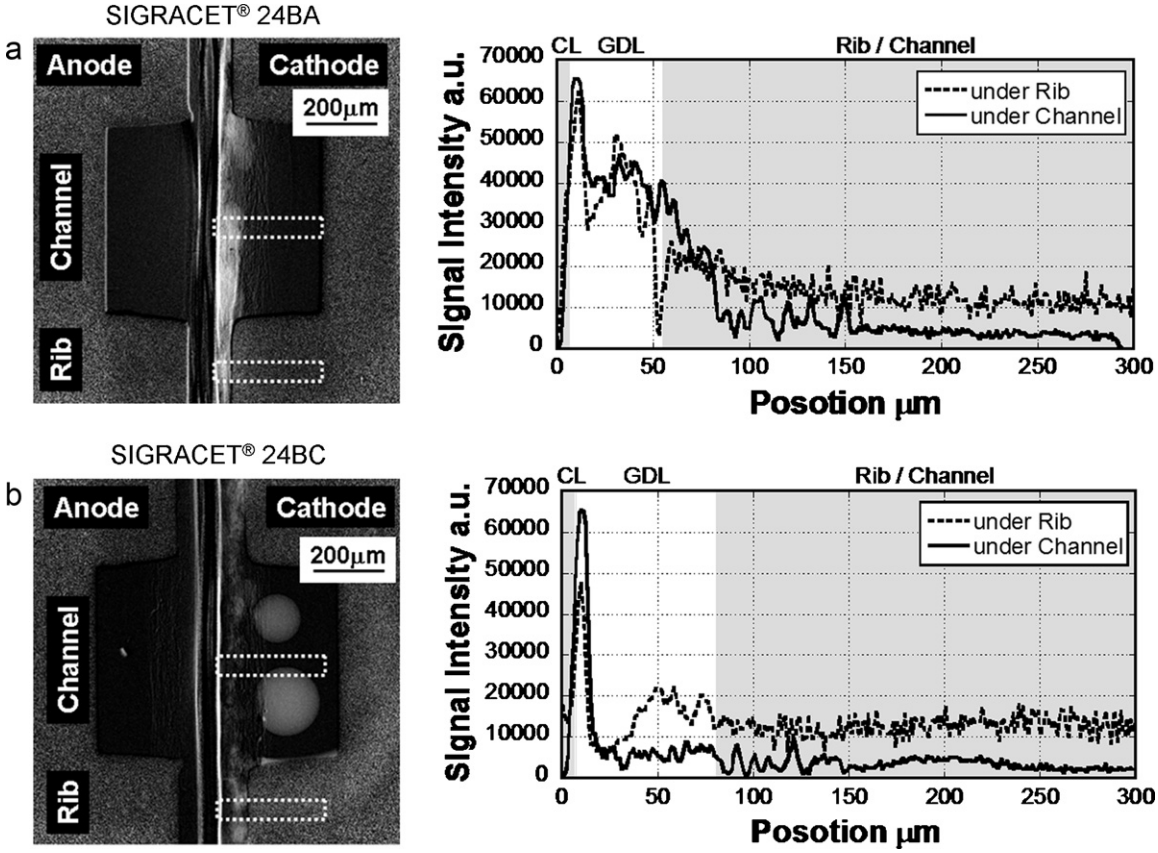

Fig. 8. One-dimensional profile of liquid water under channel and rib area at the current density of 0.8 A cm^{-2}. (a) SIGRACET® 24BA; and (b) SIGRACET® 24BC.

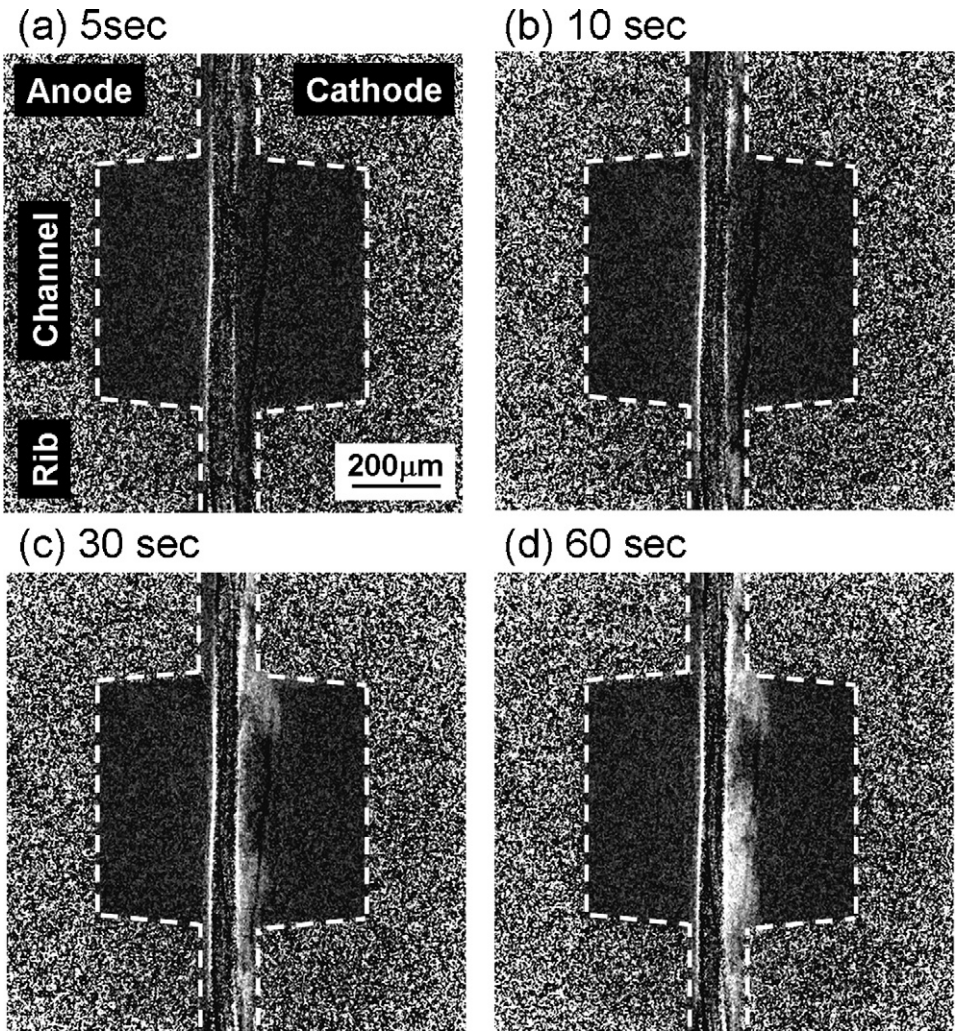

Fig. 9. Liquid water accumulation behavior in the cell with SIGRACET® 24BA at the current density of 0.8 A cm^{-2}.

LT1400-W (carbon cloth, w/MPL) were used for both the anode and the cathode GDL. The SEM images of ELAT® LT1400-W were shown in Fig. 4. Both the 24BC and the LT1400-W GDLs had the MPL, and the MPL thicknesses of these GDLs were c.a. 100 μm, but the MPL thickness of the carbon cloth GDL was not uniform.

3. Results and discussion

3.1. Image normalizing process

Fig. 5 shows the original images of the cross-sectional visualization. In the following images, the left side is the anode and the right side is the cathode. In Fig. 5(a), rib and channel structure of the cell was clearly visualized. To investigate the liquid water distribution in the entire cell, this imaging area was appropriate. But, in this study, to investigate the liquid water behavior in the porous layers in detail, the imaging area shown in Fig. 5(b) (1.0 mm × 1.0 mm) was used, and further magnification is possible.

To clarify the liquid water in the PEMFC, the images have been normalized with respect to the empty (water free) cell. Fig. 5(c) shows the normalized image, and the liquid water was identified as bright spots (white color) in this image. Because the penetration length (the width of the PEMFC) was small enough, the liquid water in the GDLs and the water hydration of the PEM was clearly visualized. In this study, we mainly focused on the liquid water behavior in the porous layers. However, further development of the soft X-ray radiography technique will make it possible to estimate the liquid water content within the membrane and the CL.

3.2. Effect of MPL on liquid water behavior

3.2.1. Effect of MPL on cell performance

To confirm the effect of the MPL on cell performance, polarization curves were measured with the 24BA (carbon paper, w/o MPL) and the 24BC (carbon paper, w/MPL) GDLs. Fig. 6(a) showed the comparison of the polarization curves between thse GDLs. Though the cell voltage of the GDLs were almost the same for operation with oxygen, the cell voltage of the 24BA GDL for operation with air showed a significant reduction at the current density of 0.4 A cm^{-2} or higher. Fig. 6(b) shows the comparison of the oxygen gain between these GDLs. The oxygen gain is defined as the difference in the cell voltage obtained using oxygen and air at a given current density. The oxygen gain of the 24BA GDL increased markedly at the current density of 0.4 A cm^{-2} or higher. Because the oxygen gain represents the oxygen transport resistance in the PEMFC, Fig. 6(b) suggested that adding the MPL can inhibit the flooding and has a beneficial effect on the cell performance.

3.2.2. Effect of MPL on liquid water behavior

To investigate the effect of adding MPL on the liquid water behavior, visualization of the liquid water in the operating PEMFC was carried out. Fig. 7 showed the liquid water distribution in the

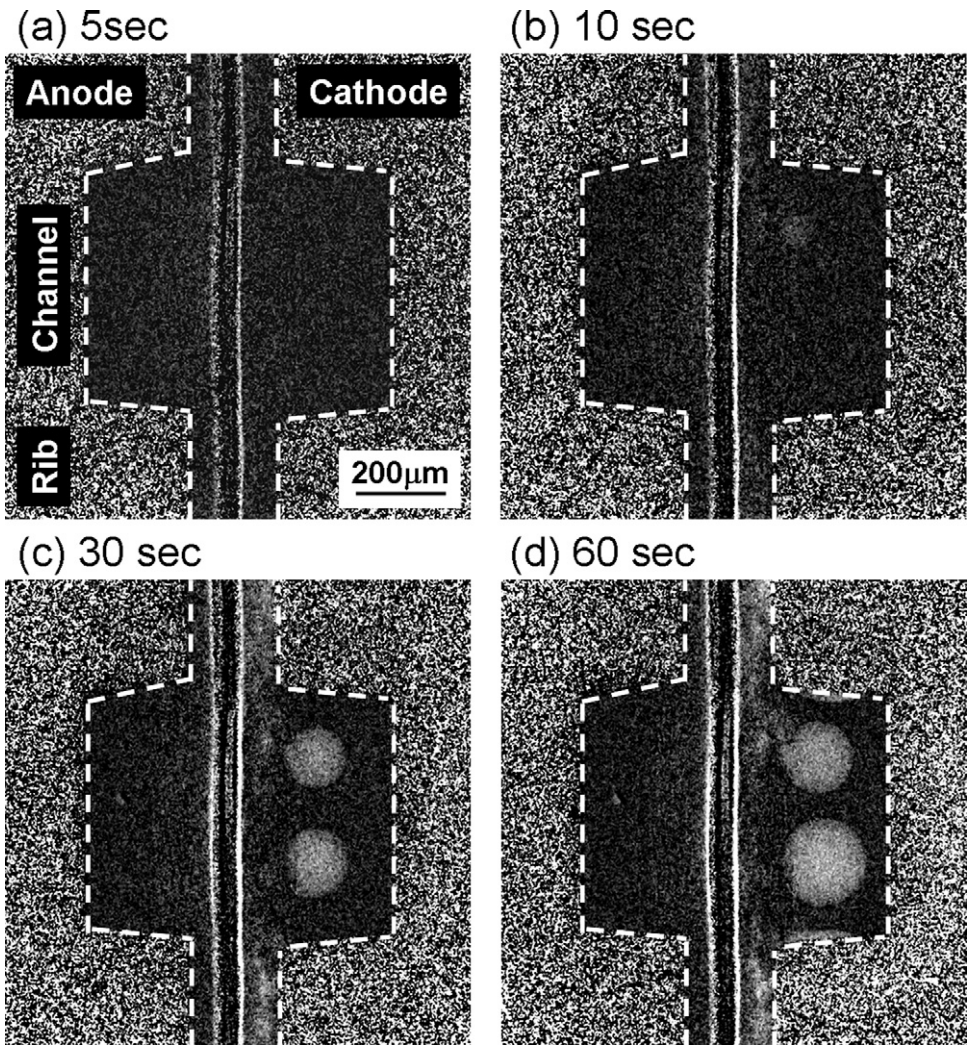

Fig. 10. Liquid water accumulation behavior in the cell with SIGRACET® 24BC at the current density of 0.8 A cm^{-2}.

24BA and the 24BC GDL. Each images were obtained at 400 s after the initiation of power generation, and the amount of the liquid water in the PEMFC seemed to be in stable condition at that time. At the current density of 0.4 A cm^{-2}, the liquid water in both the 24BA and the 24BC GDLs were mainly accumulated under the rib area, and the area under the channel contained little amount of the liquid water. On the other hand, the liquid water was observed in all parts of the GDL at the current density of 0.8 A cm^{-2}. Because of the longer diffusion length for the area under the ribs, it was conduced to a less effective liquid water removal into the vapor phase. This is the reason why the accumulation of the liquid water began from the area under the rib, but it must be noted that this is the only one possible explanation, and other phenomena, such as local changes in temperature and current density, may also play a significant role in liquid water distribution. Fig. 8 shows the one-dimensional profile of the liquid water at the current density of 0.8 A cm^{-2}. In this figure, the liquid water profiles under the cathode rib and the cathode channel area were shown, and it was clearly observed that the amount of liquid water accumulated in the 24BC GDL was lower than that of the 24BA GDL. Because the MPL is highly hydrophobic layer, the liquid water cannot easily penetrate through the MPL, and the MPL can limit the access of liquid water to the substrate layer. These results suggest that the area under the rib was completely flooded with the liquid water under high current density operation, and the amount of liquid water under the channel area would significantly affect the cell performance. In addition, the liquid water discharge behaviot from the 24BC GDL was observed. Because the MPL intruded into the substrate layer of the 24BC GDL, the effective thickness of the substrate layer was slightly different between the 24BA and the 24BC GDLs (Fig. 4), and it might help to discharge the liquid water as liquid water droplet. Though the liquid water droplet in the channel directly affect the gas supply to the catalyst site, the interaction between the liquid water behavior in the channel and the cell performance is not clear yet, and further investigation is required [25]. These might be the reason why the amount of the liquid water in the 24BC GDL was lower than that of the 24BA GDL.

To investigate the effect of the MPL on the liquid water behavior in more detail, Figs. 9 and 10 showed the liquid water distribution in the 24BA and the 24BC GDLs after 5, 10, 30, and 60 s after the initiation of power generation (current density: 0.8 A cm^{-2}), respectively. In Figs. 9(a) and 10(a), the liquid water was only observed at the interface between the CL and the GDL. Because of the hydrophilic nature of the electrode pores, the liquid water tend to be accumulated at the CL/GDL interface. The liquid water accumulation at the CL/GDL interface was also observed in Fig. 8, and Hartnig et al. [26] reported the similar results obtained by the synchrotron X-ray radiography. Swamy et al. [27] reported that the CL/MPL interfacial morphology (include the cracks) might has the significant effect on the liquid water transport in the PEMFC, and

further investigation on the effect of surface morphology is required [28]. In Figs. 9(b–d) and 10(b–d), it was clearly visualized that the liquid water accumulation began from the area under the rib and spread to the area under the channel.

From these results, it is suggested that the MPL functions as a capillary barrier that prevents the liquid water in the large pores of the substrate layer from contacting and forming liquid water films on the CL. Moreover, the MPL provides the in-plane oxygen diffusion path around the localized liquid water blockages in the substrate layer, and it made possible to maintain the cell performance under high current density operation.

3.3. Effect of GDL microstructure on liquid water behavior

3.3.1. Effect of GDL microstructure on cell performance

To confirm the effect of the GDL microstructure on cell performance, polarization curves were measured with the 24BC GDL (carbon paper, w/MPL) and the LT1400-W (carbon cloth, w/MPL) GDLs. Fig. 11(a) showed the comparison of the polarization curves between the carbon paper and the carbon cloth GDLs. Even when the measurements were performed with oxygen gas, the cell voltage of the carbon paper GDL showed the small reduction of cell voltage at the current density of 0.5 A cm^{-2} or higher. Because the cell voltages of the carbon paper (the 24BA and the 24BC) GDLs were almost same for the operation with oxygen, the difference of the cell voltage between the carbon paper and the carbon cloth GDLs might be caused by the difference of the liquid water behavior in the PEMFC. Fig. 11(b) showed the oxygen gain of these GDLs. Though the difference of the oxygen gain between these GDLs were relatively small, you have to keep it in mind that the oxygen gain of the carbon paper GDL might underestimate the effect of liquid water behavior on cell performance. From the standpoint of cell performance (Fig. 11(a)), the carbon cloth GDL was less influenced by the liquid water than the carbon paper GDL.

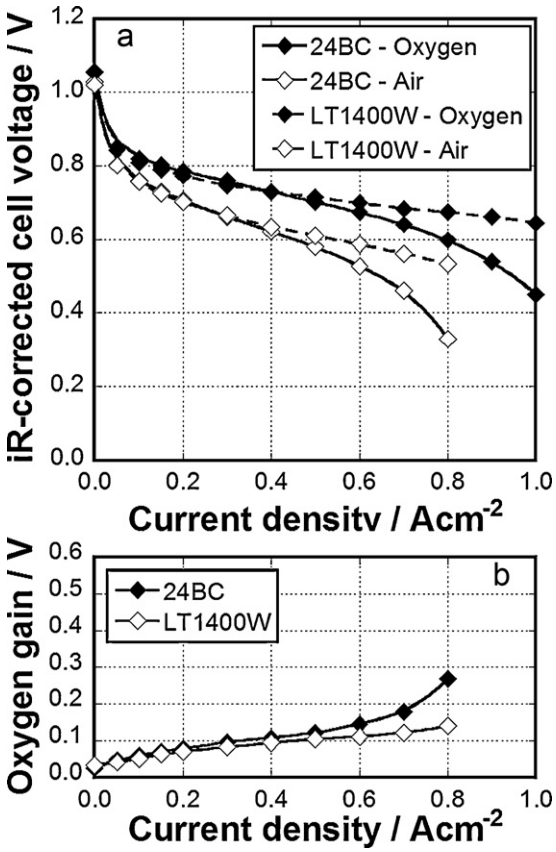

Fig. 11. Effect of the GDL microstructure on cell performance. (a) Polarization characteristics; and (b) oxygen gain.

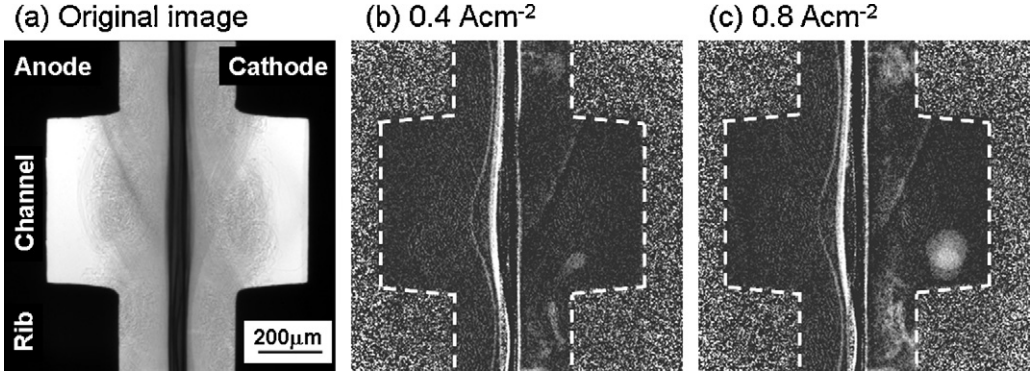

Fig. 12. Effect of current density on liquid water distribution in MEA.

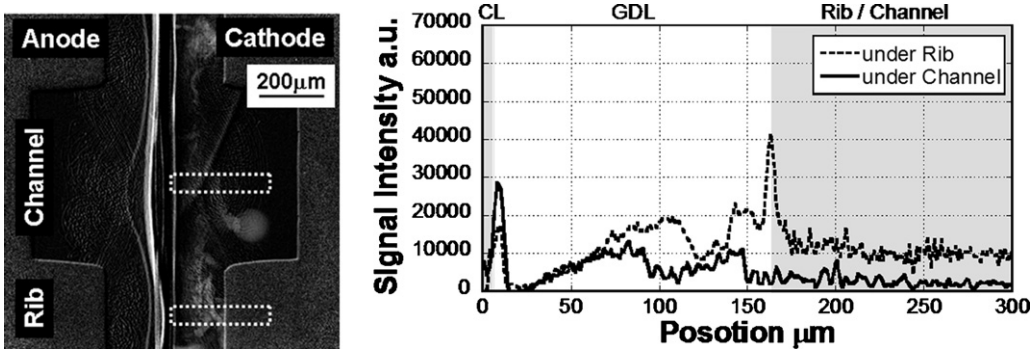

Fig. 13. One-dimensional profile of liquid water under channel and rib area with ELAT® LT1400-W at the current density of 0.8 A cm^{-2}.

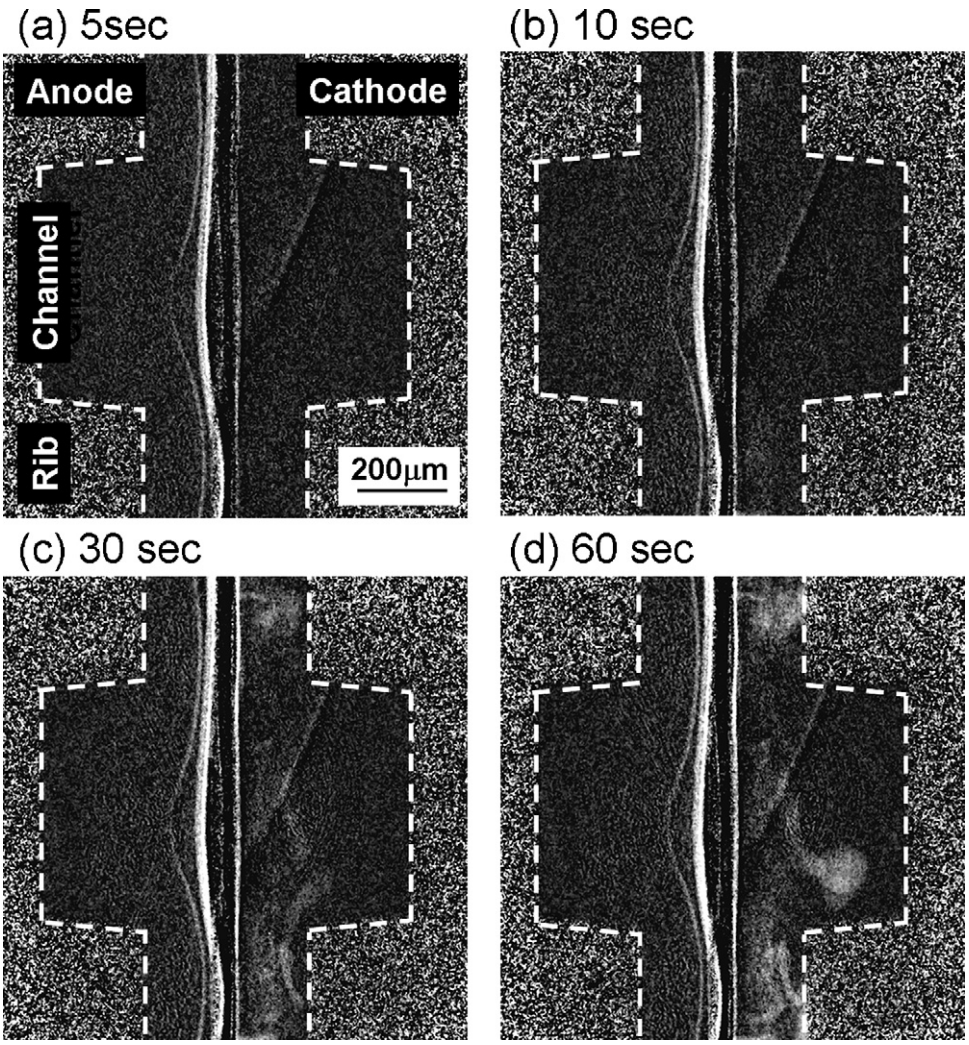

Fig. 14. Liquid water accumulation behavior in the cell with ELAT® LT1400-W at the current density of 0.8 A cm^{-2}.

3.3.2. Effect of GDL microstructure on liquid water behavior

To investigate the effect of the GDL microstructure on the liquid water behavior, visualization of the liquid water in the operating PEMFC was carried out. The visualization results of the carbon paper GDL were already shown in Figs. 7, 8 and 10. The liquid water distribution of the carbon cloth GDL at the current density of 0.4 A cm^{-2} and 0.8 A cm^{-2} was shown in Fig. 12. The liquid water in the carbon paper GDL was widely spread in the GDL, and the oxygen transport path to the reaction site seemed to be blocked by the liquid water. On the other hand, the liquid water in the carbon cloth GDL was mainly concentrated at the weaves of fiber bundle (large pore), and the small pores were kept dry. The amount of the liquid water in the PEMFC was less influenced by the current density of the cell. Fig. 13 shows the one-dimensional profile of the liquid water at the current density of 0.8 A cm^{-2}. Despite the cell performance was different between the carbon paper GDL and the carbon cloth GDL, the amount of the liquid water in the carbon cloth GDL was almost the same as that of the carbon paper GDL (Fig. 8). In the case of the carbon cloth GDL, the oxygen can diffuses through the small pores inside the fiber bundle, and this is the reason why the carbon cloth GDL can maintain the cell voltage under the high current density operation.

In addition, the liquid water accumulation and discharge behavior in the carbon cloth GDL at the current density of 0.8 A cm^{-2} was shown in Fig. 14. As mentioned above, the liquid water concentrated at the weaves of fiber bundle (large pore) was transported along the fiber bundle, and was effectively discharged to the channel. Therefore, the amount of the liquid water contained in the carbon cloth GDL was less influenced by the current density of the cell, and this is the reason why the carbon cloth GDL can maintain the oxygen transport path under high current density distribution.

From these results, the importance of the GDL microstructure on the liquid water behavior in the PEMFC was confirmed, and the detailed understanding of the porous structures (wettability, tortuosity, etc.) and the network of liquid water is essential for keeping the oxygen transport path to the catalyst site under high current density operation.

4. Conclusions

In order to investigate the effect of the microstructure of the PEMFC porous layers on liquid water transport, the visualization tests of the liquid water accumulation and discharge behavior in the operating PEMFC was carried out by laboratory-based soft X-ray radiography. The cross-sectional imaging can resolve the each components of the PEMFC, and the utilization of soft X-ray range made it possible to visualize the liquid water in the PEMFC with the spatial resolution of 0.8 μm and temporal resolution of 2.0 s frame^{-1}.

The carbon paper GDL with the MPL displayed better performance than the carbon paper GDL without the MPL. The visualization results showed that the MPL functions as a capillary barrier that prevents the liquid water in the large pores of

the substrate layer from contacting and forming the liquid water films on the hydrophilic electrode pores. With the MPL, the in-plane oxygen diffusion path around the localized liquid water blockages in the substrate layer was provided, and it made possible to maintain the cell performance under high current density operation.

The carbon cloth GDL displayed better performance than the carbon paper GDL under high current density operation. The liquid water in the carbon cloth GDL was concentrated at the weaves of fiber bundle (large pore), and was effectively discharged to the channel. The oxygen can diffuse through the small pores inside the fiber bundle, and this is the reason why the carbon cloth GDL can keep maintain the cell voltage under the high current density operation.

These observation results suggested that the microstructure of the PEMFC porous layers strongly affect the liquid water behavior in the operating PEMFC, and the detailed understanding of the porous structures (wettability, tortuosity, etc.) and the network of liquid water is essential for keeping the oxygen transport path to the catalyst site under high current density operation.

Acknowledgment

The authors acknowledge financial support for this research work from the New Energy and Industrial Technology Development Organization (NEDO), Japan.

Appendix A. Supplementary data

Supplementary data associated with this article can be found, in the online version, at doi:10.1016/j.jpowsour.2011.05.045.

References

[1] C.Y. Wang, Chem. Rev. 104 (2004) 4727–4766.
[2] U. Pasaogullari, C.Y. Wang, J. Electrochem. Soc. 152 (2005) A380–A390.
[3] A.Z. Weber, J. Newman, Chem. Rev. 104 (2004) 4679–4726.
[4] G. Lin, W. He, T.V. Nguyen, J. Electrochem. Soc. 151 (2004) A1999–A2006.
[5] P.K. Sinha, P.P. Mukherjee, C.Y. Wang, J. Mater. Chem. 17 (2007) 3089–3103.
[6] P.P. Mukherjee, C.Y. Wang, Q. Kang, Electrochim. Acta 54 (2009) 6861–6875.
[7] G. Inoue, Y. Matsukuma, M. Minemoto, ECS Trans. 25 (2009) 1519–1527.
[8] F.Y. Zhang, X.G. Yang, C.Y. Wang, J. Electrochem. Soc. 153 (2006) A225–A232.
[9] D. Spernjak, A.K. Prasad, S.G. Advani, J. Power Sources 170 (2007) 334–344.
[10] J. Zhang, D. Klamer, R. Shimoi, Y. Ono, E. Lehmann, A. Wokaun, K. Shinohara, G.G. Scherer, Electrochim. Acta 51 (2006) 2715–2727.
[11] M.A. Hickner, N.P. Siegel, K.S. Chen, D.S. Hussey, D.L. Jacobson, M. Arif, J. Electrochem. Soc. 155 (2008) B427–B434.
[12] P. Boillat, D. Kramer, B.C. Seyfang, G. Frei, E. Lehmann, G.G. Scherer, A. Wokaun, Y. Ichikawa, Y. Tasaki, K. Shinohara, Electrochem. Commun. 10 (2008) 546–550.
[13] D.S. Hussey, E. Baltic, D.L. Jacobson, ECS Trans. 33 (2010) 1385–1395.
[14] P.K. Sinha, P. Halleck, C.Y. Wang, Electrochem. Solid-State Lett. 9 (2006) A344–348.
[15] T. Koido, T. Furusawa, K. Moriyama, J. Power Sources 175 (2008) 127–136.
[16] I. Manke, C. Hartnig, M. Grunerbel, W. Lehnert, N. Kardjilov, A. Haibel, A. Hilger, J. Banhart, H. Riesemeier, Appl. Phys. Lett. 90 (2007), 174105–174105-3.
[17] C. Hartnig, I. Manke, R. Kuhn, S. Kleinau, J. Goebbels, J. Banhart, J. Power Sources 188 (2009) 468–474.
[18] T. Sasabe, S. Tsushima, S. Hirai, Int. J. Hydrogen Energy 35 (2010) 11119–11128.
[19] A.Z. Weber, J. Newman, J. Electrochem. Soc. 152 (2005) A677–A688.
[20] Y. Fujii, S. Tsushima, S. Hirai, ECS Trans. 25 (2009) 1783–1789.
[21] H.K. Atiyeh, K. Karan, B. Peppley, A. Phoenix, E. Halliop, J. Pharoah, J. Power Sources 170 (2007) 111–121.
[22] D. Malevich, E. Halliop, B.A. Peppley, J.G. Pharoah, K. Karan, J. Electrochem. Soc. 156 (2009) B216–B224.
[23] T. Sasabe, S. Tsushima, S. Hirai, ECS Trans. 33 (2010) 1413–1422.
[24] M. Reum, S.A. Freunberger, A. Wokaun, F.N. Büchi, J. Electrochem. Soc. 156 (2009) B301–B310.
[25] S.K. Lee, K. Ito, K. Sasaki, ECS Trans. 33 (2010) 1457–1463.
[26] C. Hartnig, I. Manke, R. Kuhn, N. Kardjilov, J. Banhart, W. Lehnert, Appl. Phys. Lett. 92 (2008) 134106–134108.
[27] T. Swamy, E.C. Kumbur, M.M. Mench, J. Electrochem. Soc. 157 (2010) B77–B85.
[28] T. Sasabe, P. Deevanhxay, S. Tsushima, S. Hirai, Electrochem. Commun 13 (2011) 638–641.